Journal of Biomechanics 48 (2015) 1490–1498

Contents lists available at ScienceDirect

Journal of Biomechanics

journal homepage: www.elsevier.com/locate/jbiomech
www.JBiomech.com

Predicted loading on the menisci during gait: The effect of horn laxity

Trent M. Guess [a,*], Swithin Razu [a], Hamidreza Jahandar [a], Antonis Stylianou [b]

[a] University of Missouri, Department of Physical Therapy, Department of Orthopaedic Surgery, 801 Clark Hall, Columbia, MO 65211-4250, United States
[b] University of Missouri Kansas City, Kansas City, MO, United States

ARTICLE INFO

Article history:
Accepted 31 January 2015

Keywords:
Menisci
Meniscal extrusion
Musculoskeletal model
Gait
Knee
Computational biomechanics

ABSTRACT

Radiographic measurements have established a link between meniscus extrusion and meniscus degeneration as well as with knee osteoarthritis. The presented work combines medical imaging with motion capture data from two healthy female subjects to create subject specific knee models that predict tibio-menisco-femoral contact forces and ligament forces during muscle driven simulations of barefoot gait. The developed computational models were used to explore the relationship between the extent of meniscal extrusion and biomechanical function by altering the laxity of the meniscal horn attachments during gait. The extrusion distance increased as laxity increased and the amount of contact force transferred through the menisci during gait decreased rapidly as the meniscal attachments became more lax. Horn attachment lengths that were 20% longer than MRI attachment lengths resulted in an almost complete loss of force transfer through the menisci during the gait cycle. Relatively small changes (2–3 mm) in the lengths at which horn bundles first become taut, manifested in large changes in the capacity of the tissue to transmit forces. As meniscal horn attachment laxity increased from 80% to 120% of the MRI measured horn distance, medial meniscus extrusion increased 3.9 mm for the first subject and 2.7 mm for the second subject. For the same horn laxity changes, the percent of medial tibiofemoral contact force transmitted through the medial meniscus during early stance decreased from 51% to 8% and from 36% to 14% for the two subjects. The results of our study show that increased meniscal extrusion occurs with increased laxity of the meniscal tibia attachments and this increased laxity results in loss of meniscal function.

© 2015 Elsevier Ltd. All rights reserved.

1. Introduction

The knee joint, situated at the center of the kinetic chain spanning the foot to the pelvis, is the largest articulation in the human body. The knee bears loads several times body weight during locomotion and experiences complex multidirectional and time varying forces during activities of daily living. The geometric constraint of the tibiofemoral joint is minimal and knee stability is therefore achieved by soft tissue structures such as the anterior and posterior cruciate ligaments, the medial and lateral collateral ligaments, the menisci, the joint capsule and the musculature that surrounds the joint (DeFrate et al., 2004; Chhabra et al., 2006; Defrate et al., 2007; LaPrade et al., 2007; Levangie and Norkin, 2011). The menisci play a crucial biomechanical role in knee function that is not completely understood. The menisci transmit tibiofemoral loads, reduce pressure on articular surfaces, provide shock absorption, and improve joint congruity (Kurosawa et al., 1980; Ahmed and Burke, 1983; Rath and Richmond, 2000). Meniscus injury, meniscectomy, and excessive meniscal translations are known pathways to cartilage degeneration and increased risk of osteoarthritis (Stehling et al., 2012; Roos et al., 1998; Beillas et al., 2007). Understanding the in vivo loading conditions and tissue interactions during activities of daily living is important in improving the design and outcomes of therapeutic interventions as well as implementation of effective engineered, prosthetic, or allograft replacements.

Most studies exploring the biomechanical function of the menisci can be classified using three approaches: 1) cadaveric, 2) radiographic, and 3) computational. Cadaver studies provide valuable information on tibio-menisco-femoral contact mechanics (Lee et al., 2006; Gilbert et al., 2014), but these studies do not necessarily replicate the in vivo physiological loading and motion produced through muscle driven ambulation. In addition, the sensors used to measure contact pressure can alter joint contact mechanics. Radiographic studies provide in vivo morphologic information of joint anatomy that offers insight to meniscus function. For example, meniscus extrusion occurs when the meniscus body extends beyond the tibial margin. The extent of meniscus extrusion has been strongly associated with meniscal degeneration (Costa et al., 2004) and knee osteoarthritis (Gale et al., 1999; Berthiaume et al., 2005; Stehling et al., 2012; Badlani et al., 2013; Wenger et al., 2013). Computational models can predict deformation of knee tissue in

* Corresponding author. Tel.: +1 573 882 1734.
E-mail address: guesstr@health.missouri.edu (T.M. Guess).
URL: http://www.mizzoumotioncenter.com (T.M. Guess).

http://dx.doi.org/10.1016/j.jbiomech.2015.01.047
0021-9290/© 2015 Elsevier Ltd. All rights reserved.

response to applied loading and several models of the knee that include meniscus–cartilage contact have been developed in the finite element (FE) framework (Beillas et al., 2004, Pena et al., 2006; Yao et al., 2006; Zielinska and Donahue, 2006; Beillas et al., 2007; Papaioannou et al., 2008). But, FE analysis is complex and computationally intensive, therefore FE models typically do not include representation of individual muscles and the analysis of contact mechanics is restricted to simplified joint boundary conditions corresponding to a discrete flexion angle and compressive joint force. Multibody dynamics, which relates the motion and forces acting on rigid bodies, is used in musculoskeletal models of movement. Simulations that predict the coordination of muscle forces that produce movement usually represent the knee as a simple one degree-of-freedom hinge joint (Sasaki and Neptune, 2010; Modenese et al., 2011). When six degree-of-freedom anatomically based tibiofemoral joints are included, multibody musculoskeletal models can be used to concurrently estimate muscle, ligament, and cartilage contact forces. However, a review of published three-dimensional multibody models of the natural knee revealed that the menisci are not included (Blankevoort et al., 1991; Pandy et al., 1998; Bei and Fregly, 2004; Caruntu and Hefzy, 2004).

The presented work combines medical imaging with motion capture data from two healthy female subjects to create subject specific knee models that predict tibio-menicso-femoral contact forces and ligament forces during muscle driven simulations of barefoot gait. Radiographic studies have established a link between meniscus extrusion and knee osteoarthritis. The developed computational models are used to explore the relationship between the extent of meniscal extrusion and biomechanical function by altering the zero-load length of the meniscal horn attachments during simulated gait.

2. Methods

2.1. Experimental procedures

Two adult females (Subject 1: age 20 years, height 159.5 cm, mass 59.0 kg, Subject 2: age 29 years, height 170 cm, mass 70.3 kg) free of any lower extremity problems participated in this study after providing written informed consent approved by the institution's human subjects review board. Prior to data collection, the subjects were fitted with two localizers on their dominant right leg, one on the thigh and one on the shank (Fig. 1). The localizers included two orthogonal mustard filled tubes visible during magnetic resonance imaging (MRI). The localizers were used to register the lower extremity segments to the motion capture coordinate system in the musculoskeletal models. During the MRI scans, the knee was slightly flexed (Fig. 1) and a knee coil used. After MRI, reflective markers were placed on each subject according to VICON's plug-in gait protocol. Additional markers were placed on the localizers, both feet, and left leg. Kinematic data and ground reaction forces were collected during barefoot walking trials using a VICON MX-T40 motion capture system and AMTI OR-6 force plates. Leg motion during passive movement of the knee (knee laxity test) was also recorded. During these laxity tests, an orthopedic surgeon manipulated the knee of each subject through its complete range of flexion–extension, abduction–adduction and internal–external rotations while taking care to minimize any forces applied to the leg.

The meniscal body extrusion index is a measure of meniscal extrusion that takes into account differences in knee size (Bruns et al., 2014). This index was calculated for both subjects from MRI and is defined as: [meniscus body extrusion/tibia width] × 100. The measurements were extracted from a single coronal plane MRI slice that showed the greatest area of the medial tibia spine. Meniscus body extrusion is the length of meniscus tissue not covering tibial cartilage in this MRI slice.

2.2. Computational models

The software program 3D-Slicer (www.slicer.org) was used to segment the MR images and create subject specific geometries for the right femur, tibia, patella, fibula, talus, calcaneus, midfoot, metatarsals, phalanges, and knee articular surfaces, menisci and ligaments. To register the bone geometries to the motion capture system, the outer skin surface geometries and mustard filled tubes of the localizers were also segmented. The software Geomagic Studio (Geomagic, Inc., Research Triangle Park, NC, USA) was used to smooth and decimate the final geometries. Generic musculoskeletal models were created using a method similar to that previously described (Guess et al., 2014). The models were developed in the commercially available multibody dynamic analysis program ADAMS (MSC Software Corporation, Santa Ana, CA) and the generic musculoskeletal models were comprised of 21 rigid body segments, 53 revolute joints, and 43 right leg muscles (Delp et al., 1990). Subject height, weight, and gender were used to scale the generic joint center locations as well as mass and inertia properties of each body segment using regression equations from the US Air Force's Generator of Body Data (GEBOD) (Cheng et al., 1994). Subject height was also used to scale muscle origin, insertion, and via point locations for the right leg. Three orthogonal revolute joints were defined at each joint center with the exception of the ankle and the metatarsophalangeal joint between the foot and toes. The metatarsophalangeal joint was modeled with a single revolute joint and the ankle was comprised of two hinge joints defining the talocrural and the talocalcaneal axes (Isman and Inman, 1968). Also, the joint between the head and neck was made rigid as head motion was not measured for this study.

The generic musculoskeletal models included locations for the plug-in gait marker set. A motion constraint was defined at each marker location and a three-axis spring was located between the motion constraints and corresponding body segment. The three-axis springs allowed movement of the rigid body bones relative to the motion constraints. Each generic model was then simulated into a static trial position where the subjects stood in a "T" pose. The motion constraints for the localizers as well as the extra leg and foot markers were added to the model according to motion capture position data. Markers defining the generic plug-in gait locations were then adjusted according to forces in the springs connecting the motion constraints to the model. This process was repeated until the spring forces were minimized. Bone geometries for each subject were then added to the static pose of each model. The cylinders of the

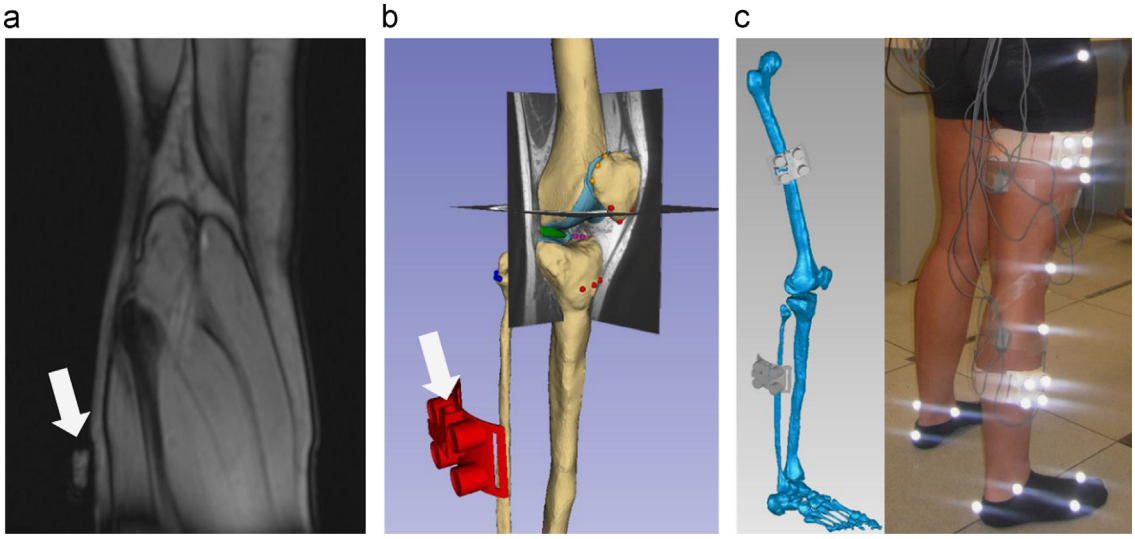


Fig. 1. Localizers on the upper and lower leg are worn by both subjects during MRI and motion capture measurements. The localizers have mustard filled tubes that are visible in MRI (a). The tubes allow placement of localizer geometries relative to the bone geometries (b). Motion capture reflective markers are attached to the localizers in known locations placing the localizers in the motion capture coordinate system (c).

Table 1
Stiffness values for the tibiofemoral ligament bundles.

Ligament bundle	Stiffness parameter (N)
ACL – anteromedial	6200
ACL – posterolateral	3400
PCL – anterolateral	12,500
PCL – posteromedial	1500
LCL – anterior	2000
LCL – middle	2000
LCL – posterior	2000
MCL – anterior superficial	2500
MCL – middle superficial	2600
MCL – posterior superficial	2700
MCL – anterior deep	1500
MCL – posterior deep	1500

localizer tubes were used to place the femur and tibia bones relative to the localizers. Motion capture markers, particularly those at palpable bone locations (e.g. malleolus), and skin geometries were also used to position the bones of the right leg. After bone placement, the joint center locations were adjusted to match actual bone geometries. Joint center locations on the left leg mirrored that of the right leg and the revolute joints for the right knee were removed.

After placement of the bone geometries, cartilage geometries were added and contacts defined between the medial and lateral tibia cartilage and femur cartilage via a compliant contact defined as:

$$F_c = k\delta^n + B(\delta)\dot{\delta} \tag{1}$$

where F_c is the contact force, δ is the interpenetration of the contacting geometries, $\dot{\delta}$ is the velocity of interpenetration, k is the contact stiffness, n is the nonlinear power exponent, and $B(\delta)$ is a damping coefficient. The values used in this model were derived from a previous study that compared contact predictions to an identically loaded finite element analysis (Guess et al., 2010) and were $k = 327\ \mathrm{N/mm^n}$, $n = 2.07$, and $B = 5\ \mathrm{Ns/mm}$.

The ligaments were attached to the bones according to the origin and insertion sites identified from the MRI. The anterior cruciate ligament (ACL) and posterior cruciate ligament (PCL) were both separated into two bundles (Duthon et al., 2006; Osti et al., 2012). The lateral collateral ligament (LCL) was separated into three bundles (Park et al., 2005) and the medial collateral ligament (MCL) was separated into five bundles, three superficial and two deep bundles (Liu et al., 2010; Liu et al., 2011; Hartshorn et al., 2013). Each ligament was modeled as a tension only nonlinear spring using a piecewise function (Blankevoort and Huiskes, 1991) that describes the force–length relationship of each bundle. The ligament strain ϵ is defined as in Eq. (2), where l is the length of the ligament after deformation and l_0 is the zero-load length. The ligament force–length relationship is quadratic for strains less than $2\epsilon_l$, where ϵ_l is assumed to be 0.03, and linear for strain values above $2\epsilon_l$ (Eq. 3). In Eq. (3), k is a stiffness parameter unique to each bundle (Table 1) and obtained from the literature (Blankevoort and Huiskes, 1991; Robinson et al., 2005; Woo et al., 2006, Petersen and Zantop, 2007; Bowman and Sekiya, 2009)

$$\epsilon = (l - l_0)/l_0 \tag{2}$$

$$f = \begin{cases} \frac{1}{4}k\epsilon^2/\epsilon_l & 0 \le \epsilon \le 2\epsilon_l \\ k(\epsilon - \epsilon_l) & \epsilon > 2\epsilon_l \\ 0 & \epsilon < 0 \end{cases} \tag{3}$$

After addition of the ligament models, kinematic data from the experimental laxity test (which manipulated each knee through its full laxity range of motion) was applied to the motion constraints of the right leg. These laxity simulations were used for fine adjustment of the femur and tibia position and to determine the zero-load lengths of each ligament bundle. The patella was then added to the knee and a contact was defined between patella cartilage and femur cartilage using Eq. (1). The lateral and medial patellofemoral ligaments were represented using Eqs. (2) and (3) with three bundles for the medial and lateral sides. Zero-load lengths for the patellofemoral ligaments were determined from insertion to origin distances in the MRI position. The quadriceps muscles were modified to insert on the patella with Eqs. (2) and (3) used to represent the patellar tendon using three bundles. Zero-load lengths for the patellar tendon bundles were also determined form the MRI position and a stiffness parameter of 3500 N was used for each bundle (Hashemi et al., 2005).

The foot–ground interface was modeled for the barefoot subjects by dividing MRI derived skin geometries into five rigid bodies (Fig. 2). The heel and mid-foot skin geometries attach to the foot bone segment and the balls of the feet and toes attach to the toe bone segment via six-axis springs. Deformable contacts were defined between each foot skin rigid body and force plate or floor surface that it comes in contact with using Eq. (1) (k=50 N/mm (Lebiedowska et al., 2009)).

The menisci were modeled as multiple wedge shaped rigid bodies connected by 6 × 6 stiffness matrices (Fig. 3). The medial and lateral menisci were sectioned at 10 degree intervals radiating from the geometric center of each meniscus. For the two subjects, the medial meniscus was divided into 19 and 20 rigid bodies and the lateral meniscus was divided into 25 rigid bodies for both subjects. Mass properties were assigned to each meniscus element based on its volume and a density of 1100 kg/m^3. Each meniscus rigid body was connected to neighboring rigid bodies by the following stiffness matrix:

$$\begin{bmatrix} F_\theta \\ F_r \\ F_z \\ T_\theta \\ T_r \\ T_z \end{bmatrix} = \begin{bmatrix} K_\theta & K_{\theta r} & K_{\theta z} & 0 & 0 & 0 \\ K_{\theta r} & K_r & K_{rz} & 0 & 0 & 0 \\ K_{\theta z} & K_{rz} & K_z & 0 & 0 & 0 \\ 0 & 0 & 0 & T_\theta & 0 & 0 \\ 0 & 0 & 0 & 0 & T_r & 0 \\ 0 & 0 & 0 & 0 & 0 & T_z \end{bmatrix} \begin{bmatrix} \theta \\ r \\ z \\ a \\ b \\ c \end{bmatrix} \tag{4}$$

where $F_{\theta,r,z}$ and $T_{\theta,r,z}$ are the translational and torsional forces between elements acting in the circumferential, radial, and axial directions. K_θ, K_r, K_z, $K_{\theta r}$, $K_{\theta z}$, K_{rz}, T_θ, T_r, and T_z are the stiffness matrix parameters, θ, r, and z are relative translational displacements and a, b, and c are relative rotational displacements. Different stiffness matrix parameters were defined for the lateral and medial sides and the stiffness values were derived through an optimization and design of experiments approach that minimized the displacement error between identically loaded finite element and multibody menisci models (Guess et al., 2010).

The menisci were initially located in the model based on their relative position to the tibia during MRI. Each meniscus was connected to the tibia via 4 horn attachments (2 posterior and 2 anterior per meniscus). The horns were modeled as non-linear elastic elements using Eqs. (2) and (3). The zero-load length of each horn attachment was assumed to be the length from tibia origin to meniscus insertion in the MRI position. The stiffness of each horn was derived from Hauch et al. (2010) and was 2810 N, 1269 N, 2349 N, and 1486 N for the lateral anterior, lateral posterior, medial anterior, and medial posterior horn attachments respectively. The origin and insertion sites for the horns were derived from MRI and from the literature (Kohn and Moreno, 1995; Wilmes et al., 2007, 2008). The anterior intermeniscal ligament (AIML) was included and assumed to have attachments at the anterior horn of the medial meniscus and anterior margin of the lateral meniscus (Nelson and LaPrade, 2000). Mechanical properties of the AIML are unknown, and a recent study by Poh et al. (2012) has indicated that its biomechanical function may be minimal. As such, a stiffness value of 200 N was chosen for the AIML in this study.

Eq. (1) was used to define compliant frictionless contacts between each meniscus rigid body and femur cartilage and between each meniscus rigid body and its respective medial or lateral tibia cartilage geometry. Parameters for Eq. (1) were $k = 19\ N/\mathrm{mm^n}$, $n = 3.37$, and $B = 0.1\ \mathrm{Ns/mm}$ (Guess et al., 2010).

The experimental motion capture data for bare foot walking provided input to an inverse kinematics step for each model. In this step, the motion constraints moved the model via the three-axis springs connected to corresponding body segments while muscle lengths for the right leg and joint angles for the left leg and upper body are recorded. During the inverse kinematics simulations, the model is constrained by the defined joints as well as contact and ligament forces at the knee and contact forces between the feet and ground. The final simulation is a forward dynamics simulation that tracks joint angle errors for the upper body and left leg and muscle length errors for the right leg (Guess et al. 2014). The force and torque magnitudes for the muscles and joints are calculated via feedback controllers implemented in Simulink (The MathWorks, Inc., Natick, Massachusetts). During the forward dynamics simulations, ADAMS and Simulink are linked in co-simulation where ADAMS sends the current muscle lengths and joint angles to Simulink, and then Simulink sends muscle forces and torques to ADAMS for the next calculation step. To account for muscle size, the feedback controller parameters for each muscle are scaled based on physiological cross-sectional area. This muscle modeling scheme is a tracking algorithm that has predicted joint loading for multiple subjects and movements (Stylianou et al., 2013; Guess et al., 2014; Kia et al., 2014) including medial and lateral tibiofemoral loading during gait and during multiple cycles of a dual limb squat. As motion is the only input to the modeling scheme, ground reaction forces can be compared to model predictions. Ligament, menisci, and contact forces are also outputs.

To analyze the relationship among meniscus horn laxity, extrusion and biomechanical function, walking simulations (Fig. 4) were run for five versions of each model. For these model versions, the MRI determined zero-load lengths for each meniscal horn attachment was multiplied by a scalar that modified each length to be 80%, 90%, 100%, 110%, and 120% of its original MRI length.

3. Results

The meniscal body extrusion index is a measure of meniscal extrusion that takes into account differences in knee size. The meniscal body extrusion index was 2.6 and 2.3 for the medial and lateral menisci of Subject 1 and 2.4 and 1.0 for Subject 2. In their study, Bruns et al. (2014) measured the meniscal body extrusion index on 118 right knees and found the medial meniscus to have an average extrusion index of 2.6 with a standard deviation 1.4 and the lateral meniscus to have an average extrusion index of 0.9 with a

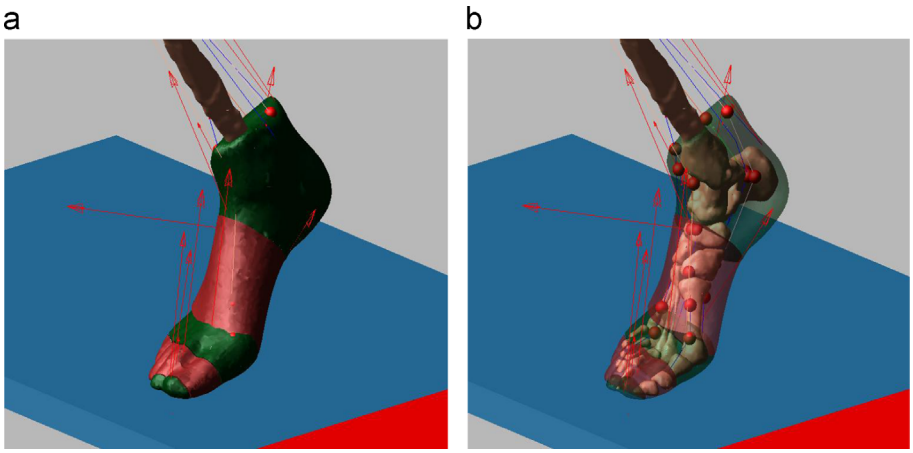


Fig. 2. Foot model. The foot skin geometry is divided into 5 rigid bodies (a). Each rigid body is connected to its respective foot bone via a 6-axis spring (b) with contacts defined between each skin geometry and the ground.

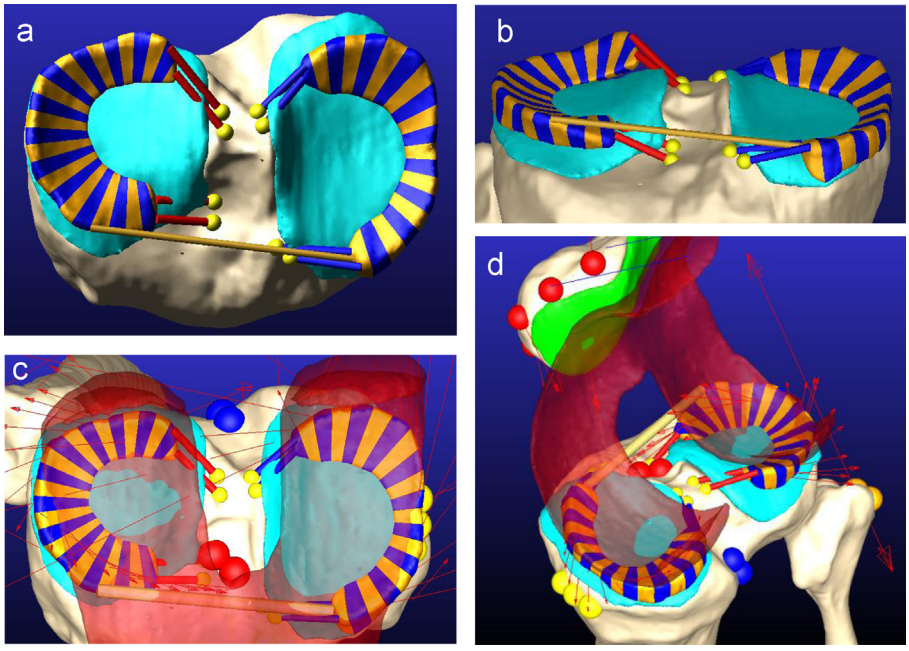


Fig. 3. Model of the multibody meniscus including 2 bundles each for the anterior and posterior horn attachments and the anterior intermeniscal ligament (AIML). The meniscus models as built from MRI derived geometries ((a) and (b)) as well as the menisci during the stance phase (c) and swing phase (d) of a forward dynamics walk simulation are shown.

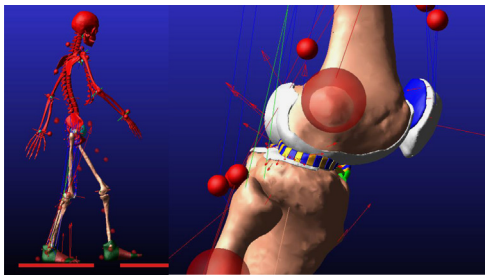


Fig. 4. Gait simulation with concurrent prediction of muscle, ligament and tibio-menisco-femoral contact forces.

standard deviation of 1.1. Both Subject 1 and Subject 2 had a medial meniscal body extrusion index within one standard deviation of the Bruns et. al. measurements and Subject 2 had a lateral extrusion index within one standard deviation. However, the lateral meniscal body extrusion index of Subject 1 was outside one standard deviation of the Bruns et. al. measurements.

Predicted ground reaction forces were comparable to measured forces (Fig. 5) with the exception of push-off, which is under predicted for both models. The ground reaction forces for the models with MRI derived meniscal horn zero-load lengths (100% model) are shown. The ground reaction forces are nearly identical for the 5 model versions for both subjects. Predicted tibiofemoral contact forces (Fig. 6) are greater for Subject 2, who was 11 kg heavier and had a slightly faster gait. The total contact force acting on the medial or lateral tibial cartilage for the 100% model is shown. Both subjects display greater contact force on the medial side with a higher ratio of medial to lateral contact force for Subject 2. The contact force patterns and magnitudes are generally consistent with contact forces measured with instrumented prosthetics (Kinney et al., 2013). The ratio of contact that only occurs between femur cartilage and tibia cartilage compared to total tibio-menisco-femoral contact force acting on either the medial or lateral tibia cartilage is presented in Fig. 7 for all models. This ratio is a measure

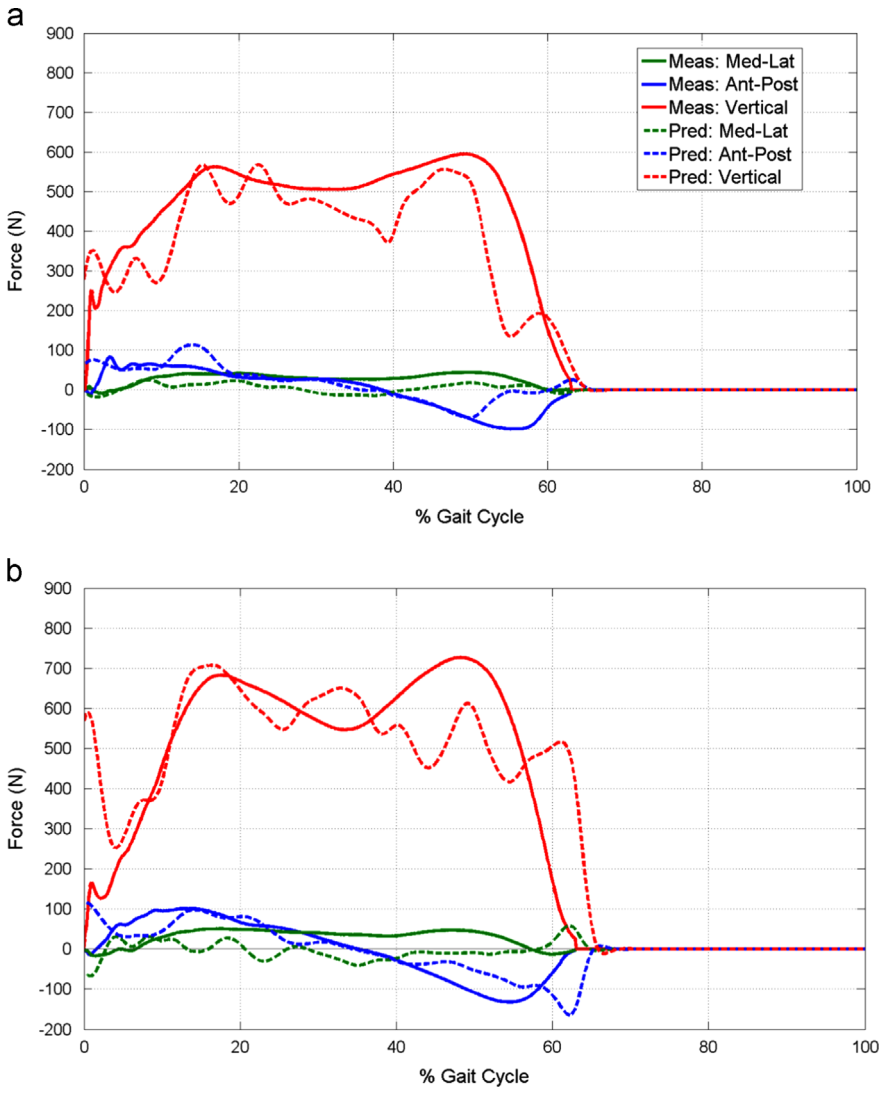


Fig. 5. Measured and predict ground reaction forces for Subject 1 (a) and Subject 2 (b)

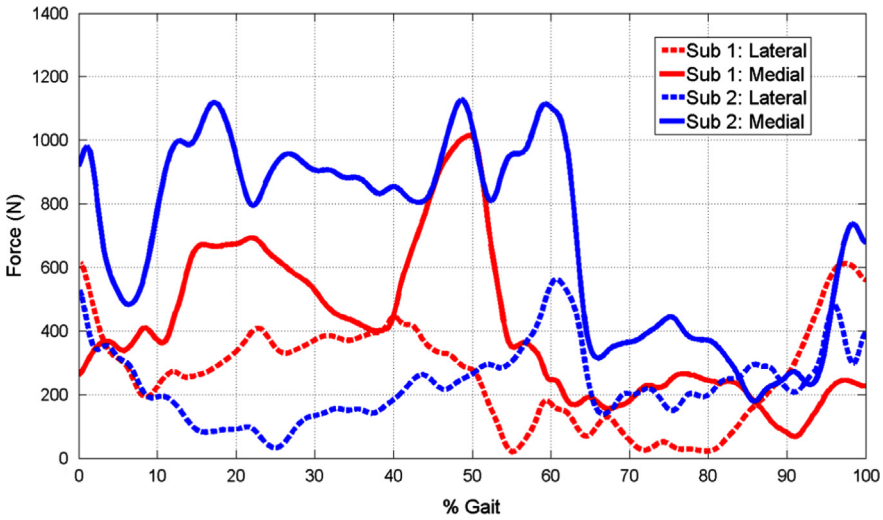


Fig. 6. Predicted contact forces during a simulated gait cycle for the lateral and medial side for Subject 1 and Subject 2.

of the force being transmitted through the menisci during a walk cycle. A ratio of 1 would indicate that no force is being transferred through the menisci and ratio of 0 would indicate that all of the tibio-menisco-femoral contact force is being transmitted through the menisci. For both subjects, this ratio approaches 1 as the meniscal horn attachment zero-load length is increased. The force ratio is lower for the medial meniscus, indicating that the menisci are transmitting more force, during early stance than mid-stance

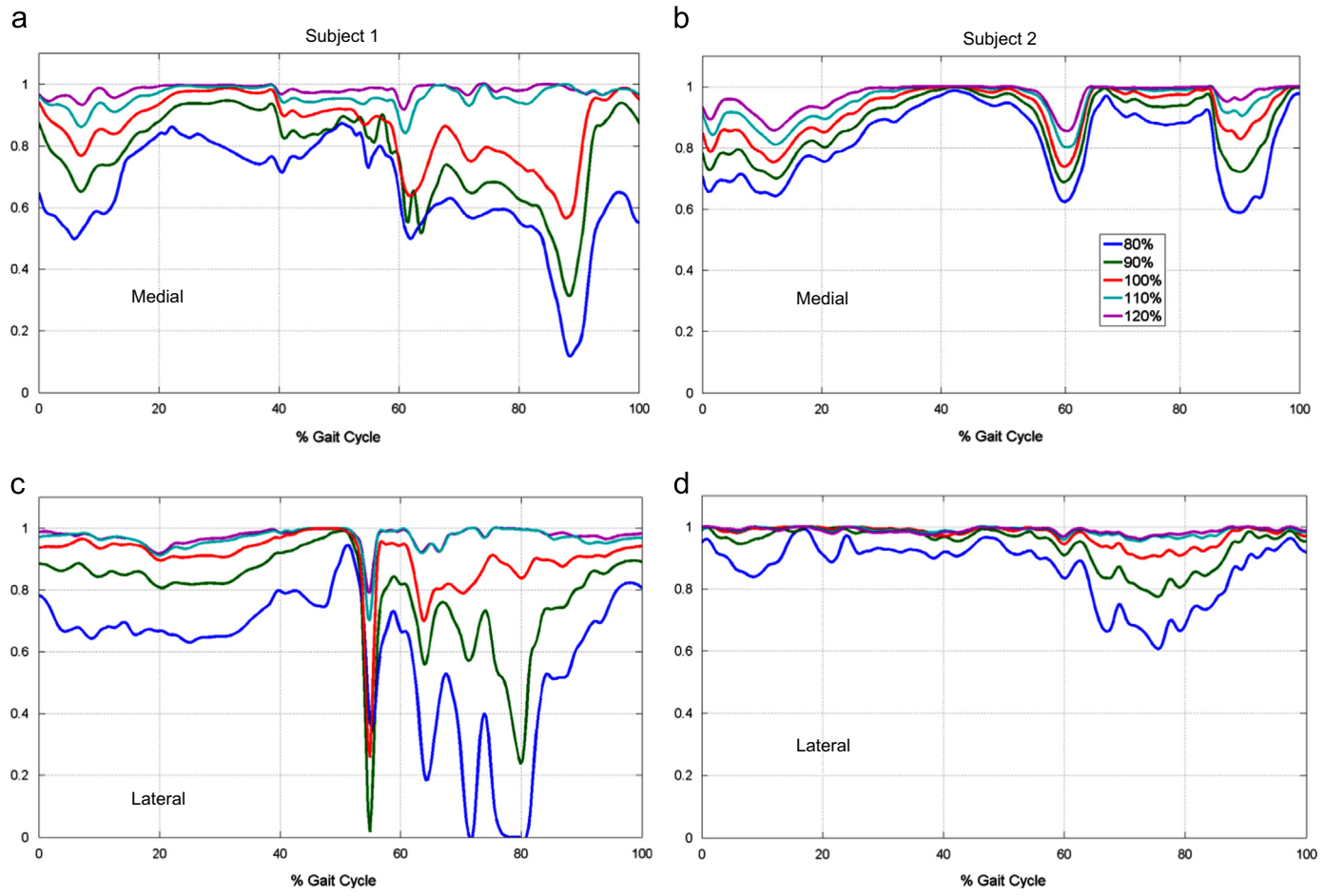


Fig. 7. Ratio of total femur cartilage to tibia cartilage contact to total contact force on a tibial plateau for medial side Subject 1 (a), lateral side Subject 1 (b), medial side Subject 2 (c), and lateral side Subject 2 (d). A ratio of one indicates that no contact force is being transmitted through the menisci and a ratio of zero indicates that all of the tibiofemoral contact force is being transmitted through the menisci.

and there is a downward peak in the ratio for the medial meniscus at 60% of gait cycle and again at 90% of gait cycle for both subjects. During swing phase, the force ratio is lower for the lateral menisci than stance phase for both subjects.

The anterior–posterior excursion of the meniscus is greater for the medial side than for the lateral side for both Subject 1 and Subject 2 (Fig. 8). The excursion of the most medial meniscus rigid body for the medial meniscus and the most lateral rigid body of the lateral meniscus (100% model) is shown. Translation of the meniscal body is measured in the local tibia coordinate system with the coordinate defined using Grood and Suntay's definition (Grood and Suntay, 1983). The excursion distance over the walk cycle in the anterior–posterior direction is 9.2 mm and 13.1 mm for the medial meniscus for Subjects 1 and 2 respectively and 6.4 mm and 8.7 mm for the lateral meniscus. Meniscal extrusion at 90% of the gait cycle is given in Table 2. The extrusion distance is defined as the distance between the outer edge of the most medial or lateral meniscal rigid body and the outer edge of the medial or lateral tibia cartilage acting along the medial–lateral axis of the local Grood and Suntay tibia coordinate. The time of 90% gait cycle is chosen for this measurement as the flex-extension angle is close to that of the MRI angle and the leg is loaded less during swing phase than during stance phase. Extrusion distance increases as laxity of the horn attachments increase.

4. Discussion

The menisci of the knee are fundamental to joint biomechanics. The menisci reduce articular cartilage contact pressures and play key roles in joint congruency, stability, load transmission, and lubrication. Detailed information on meniscus biomechanics during movement is lacking and to our knowledge, the model presented in this study is the first to combine natural knee contact mechanics, including the menisci, within muscle driven gait simulations. The biomechanical function of the menisci results from a delicate balance of geometric and mechanical properties, a balance that can be altered if any elements in the chain are compromised. For this study, we focused on the laxity of the horn attachments, predicting alterations in load distribution during muscle driven gait simulation. Relatively small changes (2–3 mm) in the lengths at which horn bundles first become taut, manifest in large changes in the capacity of the tissue to transmit forces. Although we modeled variations in the zero-load length for this study, similar changes in laxity could occur through decreases in stiffness with aging (Woo et al., 1991) and through micro-tearing of connective tissue from injury. The importance of securely attaching allograft replacement menisci is also indicated. Abat et al. (2012) found significantly higher magnitudes of meniscal extrusion when suture fixation was used to attach meniscal allografts compared to bone plug fixation. The results of our study show that increased meniscal extrusion occurs with increased laxity of the meniscal tibia attachments and this increased laxity results in loss of meniscal function.

The excursion of the menisci on the tibia plateau during walking for our models was 9.2 mm and 13.1 mm for the medial meniscus and 6.4 mm and 8.7 mm for the lateral meniscus. Information on medial and lateral menisci motion during knee flexion, particularly during load bearing is scarce (Scholes et al., 2013). Yao et. al. measured translation of the menisci centroid on 10 subjects using MRI during passive extension and flexion (Yao et al., 2008). They



Fig. 8. Excursion of the most medial or lateral meniscal rigid body during the gait cycle for Subject 1 (a) and Subject 2 (b). Translation distance is relative to a local tibia coordinate acting along its anterior–posterior axis. Positive values are anterior to the tibia coordinate and negative values are posterior to the tibia coordinate.

Table 2
Extrusion distance (in mm) of the medial and lateral menisci at 90% of the gait cycle.

Model (%)	Medial		Lateral	
	Sub 1	Sub 2	Sub 1	Sub 2
80	0.5	−0.4	−1.7	−0.1
90	0.9	0.1	−1.2	0.4
100	2.2	0.7	0.3	1.2
110	3.8	1.4	0.8	1.6
120	4.4	2.3	1.9	1.6

found that both the medial and lateral menisci translated posteriorly on the tibial plateau in deep knee flexion with the lateral meniscus moving 8.2 ± 3.2 mm and the medial meniscus moving 3.3 ± 1.5 mm. In our models, the medial menisci translate more than the lateral menisci. Applying loads to the knee does affect meniscus motion. In their MRI study, Boxheimer et al. (2004) measured 10.5 ± 3.6 mm of anterior horn motion of the medial meniscus when flexing from a supine neutral position to 90 degrees while an external rotation load was applied. During the load bearing walk cycle, the anterior–posterior meniscus excursion on the tibial plateau for both subjects is within one standard deviation of that measured by Boxheimer et. al. Although the deep bundles of the medial collateral ligament were included in our models, their attachment to the medial meniscus was not modeled. The role of the deep bundles of the medial collateral ligaments on medial meniscus stability is still in question and is a topic of a future study for our lab. LaPrade et al. (2007) report that the deep MCL is a thickening of the joint capsule deep to the superficial MCL. Due to its "stout meniscal attachment", Laprade and Wijdicks (2012) divide the deep MCL into separate functional units, the meniscofemoral and meniscotibial divisions. But, based on their cadaver study, Stein et al. (2011) concluded that the medial collateral ligament did not affect the stability of the medial meniscus. The anterior intermeniscal ligament (AIML) was included in our models. The mechanical properties of this ligament are unknown. Poh et al. (2012) found no statistically significant difference in contact pressure or contact area for either tibia plateau measured on cadaver knees after transection of the AIML. In the Poh study, a static compressive load of 1800 N was applied to the cadaver knees at full extension. For the models in our study, a relatively low stiffness value of 200 N was used for Eq. (3) and AIML forces were small, below 50 N during the walk cycles.

The menisci are mobile and deformable structures which are typically modeled using the finite element method. In our models, the menisci are represented as multiple rigid bodies connected by 6×6 stiffness matrices. For identical loading, the deformations of the multibody models mimic that of linearly elastic transversely isotropic finite element models (Guess et al., 2010). However, representation of deformable structures using multiple rigid bodies is an approximation that does not allow prediction of stress and strain internal to the meniscus tissue. Wrapping of the horns around the contours of the tibia surface (Fig. 3) was not modeled. This wrapping may have an effect on meniscus biomechanics. In addition, all eight bundles representing the zero-load lengths were all modified by the same amount. As, individual horn attachments show variation in properties (Abraham and Donahue, 2013), it may be more physiologically relevant to simulate individual alterations in zero-load lengths or stiffness properties. This type of investigation is planned for future studies. Finally, the assumption that the position of the menisci relative to the tibia during MRI gives the actual zero-load length is most likely incorrect. As modeled in Eqs. (2) and (3), the zero-load length is the position in which the bundle first begins to carry tensile loading. In the MRI, the knee is relaxed and slightly flexed with little or no muscle forces. But, the meniscal horns are still most likely taut in this position in which case the actual zero-load length would be smaller than the MRI insertion to origin distance. For example, the MRI measured horn length is approximately 13.5 mm for the anterior bundles of the medial meniscus. If 30 N of tension were acting on the bundle, then the actual zero-load length would be 12.8 mm, or 95% of the MRI length. If 4.4 N were acting on the bundle in this nonlinear region, then the actual zero-load length would be 13.23 mm, or 98% of the MRI length.

Conflict of Interest Statement

The authors have no conflicts of interest to report.

Acknowledgments

This research was funded by the National Institute of Arthritis and Musculoskeletal and Skin Diseases, Award no. 1R15AR061698.

Appendix A. Supplementary information

Supplementary data associated with this article can be found in the online version at http://dx.doi.org/10.1016/j.jbiomech.2015.01.047.

References

Abat, F., Gelber, P.E., Erquicia, J.I., Pelfort, X., Gonzalez-Lucena, G., Monllau, J.C., 2012. Suture-only fixation technique leads to a higher degree of extrusion than bony fixation in meniscal allograft transplantation. Am. J. Sports Med. 40 (7), 1591–1596.

Abraham, A.C., Donahue, T.L., 2013. From meniscus to bone: a quantitative evaluation of structure and function of the human meniscal attachments. Acta Biomater. 9 (5), 6322–6329.

Ahmed, A.M., Burke, D.L., 1983. In-vitro measurement of static pressure distribution in synovial joints—Part I: tibial surface of the knee. J. Biomech. Eng. 105 (3), 216–225.

Badlani, J.T., Borrero, C., Golla, S., Harner, C.D., Irrgang, J.J., 2013. The effects of meniscus injury on the development of knee osteoarthritis: data from the osteoarthritis initiative. Am. J. Sports Med. 41 (6), 1238–1244.

Bei, Y., Fregly, B.J., 2004. Multibody dynamic simulation of knee contact mechanics. Med. Eng. Phys. 26 (9), 777–789.

Beillas, P., Lee, S.W., Tashman, S., Yang, K.H., 2007. Sensitivity of the tibio-femoral response to finite element modeling parameters. Comput. Methods Biomech. Biomed. Eng. 10 (3), 209–221.

Beillas, P., Papaioannou, G., Tashman, S., Yang, K.H., 2004. A new method to investigate in vivo knee behavior using a finite element model of the lower limb. J. Biomech. 37 (7), 1019–1030.

Berthiaume, M.J., Raynauld, J.P., Martel-Pelletier, J., Labonte, F., Beaudoin, G., Bloch, D.A., Choquette, D., Haraoui, B., Altman, R.D., Hochberg, M., Meyer, J.M., Cline, G.A., Pelletier, J.P., 2005. Meniscal tear and extrusion are strongly associated with progression of symptomatic knee osteoarthritis as assessed by quantitative magnetic resonance imaging. Ann. Rheum. Dis. 64 (4), 556–563.

Blankevoort, L., Huiskes, R., 1991. Ligament–bone interaction in a three-dimensional model of the knee. J. Biomech. Eng. 113 (3), 263–269.

Blankevoort, L., Kuiper, J.H., Huiskes, R., Grootenboer, H.J., 1991. Articular contact in a three-dimensional model of the knee. J. Biomech. 24 (11), 1019–1031.

Bowman Jr, K.F., Sekiya, J.K., 2009. Anatomy and biomechanics of the posterior cruciate ligament and other ligaments of the knee. Op. Tech. Sports Med. 17 (3), 126–134.

Boxheimer, L., Lutz, A.M., Treiber, K., Goepfert, K., Crook, D.W., Marincek, B., Weishaupt, D., 2004. MR imaging of the knee: position related changes of the menisci in asymptomatic volunteers. Investig. Radiol. 39 (5), 254–263.

Bruns, K., Svensson, F., Turkiewicz, A., Wirth, W., Guermazi, A., Eckstein, F., Englund, M., 2014. Meniscus body position and its change over four years in asymptomatic adults: a cohort study using data from the Osteoarthritis Initiative (OAI). BMC Musculoskelet. Disord. 15, 32.

Caruntu, D.I., Hefzy, M.S., 2004. 3-D anatomically based dynamic modeling of the human knee to include tibio-femoral and patello-femoral joints. J. Biomech. Eng. 126 (1), 44–53.

Cheng, H., Obergefell, L., Rizer, A., 1994. Generator of Body Data (GEBOD) Manual. A. F. M. Command, Dayton, OH.

Chhabra, A., Starman, J.S., Ferretti, M., Vidal, A.F., Zantop, T., Fu, F.H., 2006. Anatomic, radiographic, biomechanical, and kinematic evaluation of the anterior cruciate ligament and its two functional bundles. J. Bone Joint Surg. Am. 88 (Suppl. 4), S2–S10.

Costa, C.R., Morrison, W.B., Carrino, J.A., 2004. Medial meniscus extrusion on knee MRI: is extent associated with severity of degeneration or type of tear? AJR Am. J. Roentgenol. 183 (1), 17–23.

DeFrate, L.E., Gill, T.J., Li, G., 2004. In vivo function of the posterior cruciate ligament during weightbearing knee flexion. Am. J. Sports Med. 32 (8), 1923–1928.

Defrate, L.E., Nha, K.W., Papannagari, R., Moses, J.M., Gill, T.J., Li, G., 2007. The biomechanical function of the patellar tendon during in-vivo weight-bearing flexion. J. Biomech. 40 (8), 1716–1722.

Delp, S.L., Loan, J.P., Hoy, M.G., Zajac, F.E., Topp, E.L., Rosen, J.M., 1990. An interactive graphics-based model of the lower extremity to study orthopaedic surgical procedures. IEEE Trans. Biomed. Eng. 37 (8), 757–767.

Duthon, V.B., Barea, C., Abrassart, S., Fasel, J.H., Fritschy, D., Menetrey, J., 2006. Anatomy of the anterior cruciate ligament. Knee Surg. Sports Traumatol. Arthrosc. 14 (3), 204–213.

Gale, D.R., Chaisson, C.E., Totterman, S.M., Schwartz, R.K., Gale, M.E., Felson, D., 1999. Meniscal subluxation: association with osteoarthritis and joint space narrowing. Osteoarthr. Cartil. 7 (6), 526–532.

Gilbert, S., Chen, T., Hutchinson, I.D., Choi, D., Voigt, C., Warren, R.F., Maher, S.A., 2014. Dynamic contact mechanics on the tibial plateau of the human knee during activities of daily living. J. Biomech. 47 (9), 2006–2012.

Grood, E.S., Suntay, W.J., 1983. A joint coordinate system for the clinical description of three-dimensional motions: application to the knee. J. Biomech. Eng. 105 (2), 136–144.

Guess, T.M., Stylianou, A.P., Kia, M., 2014. Concurrent Prediction of Muscle and Tibiofemoral Contact Forces During Treadmill Gait. J. Biomech. Eng. 136 (2) 021032-021032.

Guess, T.M., Thiagarajan, G., Kia, M., Mishra, M., 2010. A subject specific multibody model of the knee with menisci. Med. Eng. Phys. 32 (5), 505–515.

Hartshorn, T., Otarodifard, K., White, E.A., Hatch 3rd, G.F., 2013. Radiographic landmarks for locating the femoral origin of the superficial medial collateral ligament. Am. J. Sports Med. 41 (11), 2527–2532.

Hashemi, J., Chandrashekar, N., Slauterbeck, J., 2005. The mechanical properties of the human patellar tendon are correlated to its mass density and are independent of sex. Clin. Biomech. 20 (6), 645–652.

Hauch, K.N., Villegas, D.F., Haut Donahue, T.L., 2010. Geometry, time-dependent and failure properties of human meniscal attachments. J. Biomech. 43 (3), 463–468.

Isman, R.E., Inman, V.T., 1968. Anthropometric Studies of the Human Foot and Ankle. University of California, Biomechanics Laboratory, Berkeley.

Kia, M., Guess, T.M., Stylianou, A., 2014. Evaluation of a musculoskeletal model with prosthetic knee through six experimental gait trials. Med. Eng. Phys..

Kinney, A.L., Besier, T.F., D'Lima, D.D., Fregly, B.J., 2013. Update on grand challenge competition to predict in vivo knee loads. J. Biomech. Eng. 135 (2), 021012.

Kohn, D., Moreno, B., 1995. Meniscus insertion anatomy as a basis for meniscus replacement: a morphological cadaveric study. Arthroscopy 11 (1), 96–103.

Kurosawa, H., Fukubayashi, T., Nakajima, H., 1980. Load-bearing mode of the knee joint: physical behavior of the knee joint with or without menisci. Clin. Orthop. Relat. Res. 149, 283–290.

LaPrade, R.F., Engebretsen, A.H., Ly, T.V., Johansen, S., Wentorf, F.A., Engebretsen, L., 2007. The anatomy of the medial part of the knee. J. Bone Joint Surg. Am. 89 (9), 2000–2010.

Laprade, R.F., Wijdicks, C.A., 2012. The management of injuries to the medial side of the knee. J. Orthop. Sports Phys. Ther. 42 (3), 221–233.

Lebiedowska, M.K., Wente, T.M., Dufour, M., 2009. The influence of foot position on body dynamics. J. Biomech. 42 (6), 762–766.

Lee, S.J., Aadalen, K.J., Malaviya, P., Lorenz, E.P., Hayden, J.K., Farr, J., Kang, R.W., Cole, B.J., 2006. Tibiofemoral contact mechanics after serial medial meniscectomies in the human cadaveric knee. Am. J. Sports Med. 34 (8), 1334–1344.

Levangie, P.K., Norkin, C.C., 2011. Joint Structure and Function: A Comprehensive Analysis. F.A. Davis Company, ISBN-13: 978-0-8036-2362-0.

Liu, F., Gadikota, H.R., Kozanek, M., Hosseini, A., Yue, B., Gill, T.J., Rubash, H.E., Li, G., 2011. In vivo length patterns of the medial collateral ligament during the stance phase of gait. Knee Surg. Sports Traumatol. Arthrosc. 19 (5), 719–727.

Liu, F., Yue, B., Gadikota, H.R., Kozanek, M., Liu, W., Gill, T.J., Rubash, H.E., Li, G., 2010. Morphology of the medial collateral ligament of the knee. J. Orthop. Surg. Res. 5, 69.

Modenese, L., Phillips, A.T., Bull, A.M., 2011. An open source lower limb model: hip joint validation. J. Biomech. 44 (12), 2185–2193.

Nelson, E.W., LaPrade, R.F., 2000. The anterior intermeniscal ligament of the knee. An anatomic study. Am. J. Sports Med. 28 (1), 74–76.

Osti, M., Tschann, P., Kunzel, K.H., Benedetto, K.P., 2012. Anatomic characteristics and radiographic references of the anterolateral and posteromedial bundles of the posterior cruciate ligament. Am. J. Sports Med. 40 (7), 1558–1563.

Pandy, M.G., Sasaki, K., Kim, S., 1998. A three-dimensional musculoskeletal model of the human knee joint. Part 1: theoretical construct. Comput. Methods Biomech. Biomed. Eng. 1 (2), 87–108.

Papaioannou, G., Nianios, G., Mitrogiannis, C., Fyhrie, D., Tashman, S., Yang, K.H., 2008. Patient-specific knee joint finite element model validation with high-accuracy kinematics from biplane dynamic Roentgen stereogrammetric analysis. J. Biomech. 41 (12), 2633–2638.

Park, S.E., DeFrate, L.E., Suggs, J.F., Gill, T.J., Rubash, H.E., Li, G., 2005. The change in length of the medial and lateral collateral ligaments during in vivo knee flexion. Knee 12 (5), 377–382.

Pena, E., Calvo, B., Martinez, M.A., Doblare, M., 2006. A three-dimensional finite element analysis of the combined behavior of ligaments and menisci in the healthy human knee joint. J. Biomech. 39 (9), 1686–1701.

Petersen, W., Zantop, T., 2007. Anatomy of the anterior cruciate ligament with regard to its two bundles. Clin. Orthop. Relat. Res. 454, 35–47.

Poh, S.Y., Yew, K.S., Wong, P.L., Koh, S.B., Chia, S.L., Fook-Chong, S., Howe, T.S., 2012. Role of the anterior intermeniscal ligament in tibiofemoral contact mechanics during axial joint loading. Knee 19 (2), 135–139.

Rath, E., Richmond, J.C., 2000. The menisci: basic science and advances in treatment. Br. J. Sports Med. 34 (4), 252–257.

Robinson, J.R., Bull, A.M., Amis, A.A., 2005. Structural properties of the medial collateral ligament complex of the human knee. J. Biomech. 38 (5), 1067–1074.

Roos, H., Lauren, M., Adalberth, T., Roos, E.M., Jonsson, K., Lohmander, L.S., 1998. Knee osteoarthritis after meniscectomy: prevalence of radiographic changes after twenty-one years, compared with matched controls. Arthritis Rheum. 41 (4), 687–693.

Sasaki, K., Neptune, R.R., 2010. Individual muscle contributions to the axial knee joint contact force during normal walking. J. Biomech. 43 (14), 2780–2784.

Scholes, C., Houghton, E.R., Lee, M., Lustig, S., 2013. Meniscal translation during knee flexion: what do we really know? Knee Surg. Sports Traumatol. Arthrosc..

Stehling, C., Souza, R.B., Hellio Le Graverand, M.P., Wyman, B.T., Li, X., Majumdar, S., Link, T.M., 2012. Loading of the knee during 3.0T MRI is associated with significantly increased medial meniscus extrusion in mild and moderate osteoarthritis. Eur. J. Radiol. 81 (8), 1839–1845.

Stein, G., Koebke, J., Faymonville, C., Dargel, J., Muller, L.P., Schiffer, G., 2011. The relationship between the medial collateral ligament and the medial meniscus: a topographical and biomechanical study. Surg. Radiol. Anat. 33 (9), 763–766.

Stylianou, A.P., Guess, T.M., Kia, M., 2013. Multibody muscle driven model of an instrumented prosthetic knee during squat and toe rise motions. J. Biomech. Eng. 135 (4), 041008.

Wenger, A., Wirth, W., Hudelmaier, M., Noebauer-Huhmann, I., Trattnig, S., Bloecker, K., Frobell, R.B., Kwoh, C.K., Eckstein, F., Englund, M., 2013. Meniscus body position, size, and shape in persons with and persons without radiographic knee osteoarthritis: quantitative analyses of knee magnetic resonance images from the osteoarthritis initiative. Arthritis Rheum. 65 (7), 1804–1811.

Wilmes, P., Anagnostakos, K., Weth, C., Kohn, D., Seil, R., 2008. The reproducibility of radiographic measurement of medial meniscus horn position. Arthroscopy 24 (6), 660–668.

Wilmes, P., Pape, D., Kohn, D., Seil, R., 2007. The reproducibility of radiographic measurement of lateral meniscus horn position. Arthroscopy 23 (10), 1079–1086.

Woo, S.L., Hollis, J.M., Adams, D.J., Lyon, R.M., Takai, S., 1991. Tensile properties of the human femur-anterior cruciate ligament-tibia complex. The effects of specimen age and orientation. Am. J. Sports Med. 19 (3), 217–225.

Woo, S.L.Y., Abramowitch, S.D., Kilger, R., Liang, R., 2006. Biomechanics of knee ligaments: injury, healing, and repair. J. Biomech. 39 (1), 1–20.
Yao, J., Lancianese, S.L., Hovinga, K.R., Lee, J., Lerner, A.L., 2008. Magnetic resonance image analysis of meniscal translation and tibio-menisco-femoral contact in deep knee flexion. J. Orthop. Res. 26 (5), 673–684.
Yao, J., Snibbe, J., Maloney, M., Lerner, A.L., 2006. Stresses and strains in the medial meniscus of an ACL deficient knee under anterior loading: a finite element analysis with image-based experimental validation. J. Biomech. Eng. 128 (1), 135–141.
Zielinska, B., Donahue, T.L., 2006. 3D finite element model of meniscectomy: changes in joint contact behavior. J. Biomech. Eng. 128 (1), 115–123.